coatings

MDPI

Article

Comparative Study on Wear Behaviors of Monolayer and Heterogeneous Multilayer Ta Coatings in Atmospheric and SBF Environments

Yun Yue [1,†], Shuguang Liu [2,3,*,†], Weiwei Qiu [2], Fei Wang [2], Yongjie Xue [2], Chaoqun Xia [4] and Sanming Du [1]

[1] National United Engineering Laboratory for Advanced Bearing Tribology, Henan University of Science and Technology, Luoyang 471000, China
[2] Engineering Research Center for Electrophysical Apparatus and Application Technology, Beijing Research Institute of Automation for Machinery Industry Co., Ltd., Beijing 100120, China
[3] State Key Laboratory of Metastable Materials Science and Technology, Yanshan University, Qinhuangdao 066004, China
[4] School of Materials Science and Engineering, Research Institute for Energy Equipment Materials, Hebei University of Technology, Tianjin 300130, China
* Correspondence: liushg@riamb.ac.cn
† These authors contributed equally to this work.

Abstract: Monolayer Ta and multilayer Ti/Zr/Ta and Zr/Ti/Ta coatings were prepared by magnetron sputtering on TC4 substrates to improve the surface friction and wear properties in a simulated body fluid (SBF) environment and an atmospheric environment. Optical microscopy, scanning electron microscopy, laser scanning confocal microscopy and nano scratch testing were employed to establish the structure-property-environment relationships. By controlling the preparation parameters, the outermost layer of all three samples was Ta coating, and the total coating thickness of each sample was about 3 µm. Friction and wear testing revealed that, compared to bare TC4 substrate, and multilayer Ti/Zr/Ta and Zr/Ti/Ta coatings, the monolayer Ta possessed the lowest friction coefficient as well as the minimum wear rate (i.e., calculation result of the wear track width and wear depth). This was mainly attributed to excellent adhesion strength, a particular structure and solid lubrication of the monolayer coating. The same coating sample exhibited a stronger wear resistance in the SBF environment than in the atmospheric environment. Furthermore, the wear behaviors and mechanisms of various coatings under different experimental environments are also discussed.

Keywords: titanium alloy; tantalum coating; magnetron sputtering; friction and wear properties; wear morphology

check for updates

Citation: Yue, Y.; Liu, S.; Qiu, W.; Wang, F.; Xue, Y.; Xia, C.; Du, S. Comparative Study on Wear Behaviors of Monolayer and Heterogeneous Multilayer Ta Coatings in Atmospheric and SBF Environments. *Coatings* **2023**, *13*, 120. https://doi.org/10.3390/coatings13010120

Academic Editor: Alexander D. Modestov

Received: 9 December 2022
Revised: 29 December 2022
Accepted: 6 January 2023
Published: 9 January 2023

Copyright: © 2023 by the authors. Licensee MDPI, Basel, Switzerland. This article is an open access article distributed under the terms and conditions of the Creative Commons Attribution (CC BY) license (https://creativecommons.org/licenses/by/4.0/).

1. Introduction

Metallic biomaterials such as tantalum (Ta), zirconium (Zr), titanium (Ti) and Ti alloys have been extensively used in clinical applications [1–6]. Especially in orthopedics and stomatology, advanced material preparation technology of the metal implants used in hard tissues keep reaching new efficacies for skeletal reconstructive surgery, recently referred to as "the operation of the century" [2]. Among numerous biomedical materials, Ti-6Al-4V (TC4) alloys have been developed for artificial arthroplasty, being among the first Ti biomaterials introduced into implantable components and devices [7]. However, due to the toxicity effects caused by Al and V and poor wear resistance, the development of novel implant materials for prostheses with desirable mechanical strength, wear resistance, biocompatibility and structural biostability in physiological environments has become an urgent clinical task.

In the recent decades, Ta has been shown to be a promising material for biomedical applications owing to its impressive ductility, wear resistance, chemical inertness, acid and alkali corrosion resistance, and in vivo bioactivity. These characteristics allow Ta to

form chemical bonds with bone tissue, thereby initiating the biomineralization kinetics and optimizing the osseointegration process [8–10]. Moreover, since the 1940s, Ta has been used both in vitro and in vivo in various forms of medical instruments such as rods, wires, artificial joints, spinal fusion cages, dental implants, micro- or nano-particles, and radio markers [11]. Because of its high melting point (3017 °C), high density (16.6 g/cm^3) and the low reserves of Ta [12], it is impractical to manufacture large-scale Ta implants in the same way as Ti implants. Thus, the application of the bulk Ta implants in orthopedics and dentistry is limited by a too high specific gravity as well as the high prices of raw materials and fabrication. In order to reduce the costs and combine the mechanical properties of TC4 alloy substrate with the bioactivity of Ta metal, using Ta to modify the surface of TC4 alloy has become one of the important ways to promote the application of Ta material.

The introduction of Ta into coatings via surface modification technologies is a reliable way to improve the surface and biological properties of biomedical metallic materials [8,10,13–15]. For example, Hee et al. [15] used a filtered cathodic vacuum arc deposition technique–the so-called bio-stable surface treatment–to prepare Ta and related nitride films on TC4 alloy, after which both the Ta and TaN films exhibited improvement in corrosion resistance. Furthermore, the heterogeneous multilayer coatings are also within the scope of many studies on biocompatible materials. Echavarría et al. [14] developed a new Ta/TaN/TaN*x*(Ag)y/TaN coating system using unbalanced DC magnetron sputtering. The release of Ag to the osteoblast medium enabled one to improve the cell adhesion and differentiation of the TaN*x*(Ag)y composite coating so as to achieve an appropriate balance between biocompatibility and bacterial adhesion. Moreover, according to Ma et al. [16], Ta/TaN multilayer coatings prepared by reactive magnetron sputtering in combination with ion implantation possessed outstanding cohesive strength, wear resistance and corrosion resistance, and their service life increased 5 times compared to that of the basic material. From the above studies, it is evident that multilayer coatings demonstrate superior biological, mechanical and tribological properties compared to monolayer coatings [17]. For heterogeneous multilayer biocoating, the selection of intermediate or transition layer materials generally follows the principles of non-toxic, low cost, reduced stress level and effective barrier. Ti and Zr are biological non-toxic elements, which are expected to not only reduce the toxic ions' precipitation from the substrate but also further decrease the cost of coating preparation. Therefore, these two elements can be introduced into the multilayer coating as intermediate layers.

The tribological property of the prosthesis surface is one of the important criteria for practical application [18,19]. During surgical implantation, the prosthesis is tapped into the medullary cavity of the bone, and the friction between the prosthesis and the bone provides stability in the early implanting stage. After that, implants are inserted to realize the function of living tissues in the human body. Meanwhile, their continuous contact with tissues and body fluids produces friction and wear. In view of this, when considering wear induced coating failure, both the body fluid environment and atmospheric environment should be taken into account. However, few reports on the wear behavior of implants in atmospheric and body fluid environments have been divulged to date.

In this work, the monolayer Ta coating and the multilayer Ti/Zr/Ta and Zr/Ti/Ta coatings were prepared by magnetron sputtering on TC4 substrates. The friction-wear tests were carried out under both dry and simulated body fluid (SBF) solution conditions to compare the wear behaviors of coatings. The surface topography, microstructure, phase composition, and adhesion of the coatings were thoroughly characterized. The influence of coating structure on the tribological properties as well as the abrasion mechanisms of the coatings were investigated as well. This paper aims at a comparative study of the differences of the friction and wear behaviors / properties between the monolayer and multilayer coatings, and the same coating samples in two different environments. The research results will provide theoretical guidance for the practical application of Ta coating in the field of biomaterials.

2. Materials and Methods

2.1. Materials

The biomedical Ti alloy used in the present work was TC4 ELI alloy (hereinafter referred to as TC4) was produced by Carpenter Technology Corporation according to ASTM F136 standard. Compared to the counterparts, this TC4 alloy possessed low contents of interstitial elements (C, N, and O) and Fe as the impurity element. The TC4 alloy was processed into Ø 13 mm × 3 mm plate samples (substrates) by employing an electric spark cutting machine. The substrates were then ground with 150#, 360#, 600#, 1000#, 2000#, 3000# and 5000# SiC sandpapers. After being polished to a mirror-like surface and ultrasonically cleaned in ethanol, the substrates were put into a vacuum chamber and cleaned by argon ion etching in order to remove any surface contaminants. Subsequently, the Ti, Zr and Ta coatings were directly deposited onto the substrates by sputtering Ti (99.995%), Zr (99.9%) and Ta (99.95%) targets using a magnetron sputtering deposition system (Kurt J. Lesker PRO Line PVD). The base vacuum of the system was 2×10^{-1} Pa and the working gas was argon. The target faced the sample holder, and the sample holder allows rotation of the substrates during deposition. The deposition temperature was measured by using a thermocouple which was set at the back of a sample holder (a 2 mm thick stainless steel disc). The substrate heating temperature and sputtering power were set at 200 °C and 150 W, respectively. The applied bias voltage on the substrate was set at −90 V (direct current, DC) to obtain the monolayer Ta coating and the multilayer Ti/Zr/Ta and Zr/Ti/Ta coatings. The average deposition time of the monolayer Ta coating was 90 min, and those of Ti, Zr and Ta in the multilayer Ti/Zr/Ta and Zr/Ti/Ta coatings were approximately 90, 60 and 30 min, respectively. The outermost layers of all three coatings were Ta coatings. In addition, the working time was set at 30 min for DC. The series of produced experimental samples were labeled as TC4, Ta, Ti/Zr/Ta and Zr/Ti/Ta.

2.2. Experimental Methods

X-ray diffraction (XRD) analysis was conducted using a D/max-2500/PC diffractometer with Cu Kα radiation, and the diffractograms were recorded within the 2θ range from 20° to 100° with a step size of 0.02°. The cross-section and wear morphology of the coatings were observed in a scanning electron microscope (SEM, Hitachi SU5000, Tokyo, Japan) and an optical microscope (OM, Leica DM6000M, Wetzlar, Germany). The chemical composition was determined by means of an energy dispersive spectrometer (EDS, EDAX TEAM, Philadelphia, PA, USA) integrated in the SEM equipment. The adhesion property was evaluated via nano-scratch testing (Agilent Nano indenter G200, Santa Clara, CA, USA) using a round diamond indenter with a radius of 4.6 μm. During measurements, the load increased linearly from 0 mN to 400 mN, and the scratch length was 500 μm. The X-photoelectron spectroscopy (XPS, ESCALAB 250Xi, Waltham, MA, USA) experiments were performed on the outer surfaces of coatings to analyze the chemical bonding state therein, and the C1s signal was used as the binding energy reference. To evaluate the tribological properties of the coatings in different environments, the wear tests were conducted in a SBF solution at ambient temperature (25 ± 3 °C) using an Anton Paar Ball-on-disk tribometer TRB and in the atmospheric environment by means of a Bruker Tribometer UMT-5 (Billerica, MA, USA), respectively. During wear tests, GCr15 steel balls (Ø 6 mm) were used as the friction partners; the normal load was 2 N, the wear radius was set at 3 mm with the line speed of 5 cm/s, and the effective stop condition was 3000 laps. A laser scanning confocal microscope (Olympus LEXT OLS4100, Tokyo, Japan) was employed to assess the surface roughness of the coatings via the acquisition of wear track 2D profiles and 3D microtopography images. More details about the experimental procedure can be found in our previous study [13].

3. Results and Discussion

3.1. Structural Characteristics

Figure 1a displays the experimental XRD patterns of the samples and the standard peak positions of various common phases in pure Ti and Ta, according to ICDD/JCPDS databases. The TC4 substrate revealed a typical α + β dual-phase structure, as can be seen from the matching of the corresponding diffractogram with the standard α (PDF# 44-1294) and β (PDF# 44-1288) phase related diffraction peaks at the bottom of Figure 1a. Only the Ta-related peaks were detected in the coating samples: while the monolayer coating consisted of α-Ta (PDF# 04-0788) phase, the outermost Ta layer of the multilayer coatings mainly consisted of α-Ta with a small amount of β-Ta (PDF# 25-1280) inclusions. Generally, the α-Ta phase with a body-centered cubic lattice is stable at normal temperature and pressure, whereas the β-Ta phase with a tetragonal lattice is metastable. Gladcuk [20] and Myers [21] reported that the reduction in both persistent thermal effects and coating thickness could result in the formation of the metastable β phase. On the one hand, the non-equilibrium solidification occurred during magnetron sputtering, which is typical of this technology and is beneficial to the nucleation and growth of the metastable β-Ta phase [22]. On the other hand, it is easier to obtain the β-Ta phase when the Ta layer approaches the thin-film material. The thicker coating provides sufficient time and temperature for the equilibrium phase transition during deposition. The larger the thickness is, the more similar the coating material is to the bulk material, which is conducive to the growth of a stable phase. Therefore, the thick monolayer Ta coating consisted of the α phase, whereas the predominately stable α-Ta phase with a small number of metastable β-Ta inclusions could co-exist in the outermost layers of Ti/Zr/Ta and Zr/Ti/Ta coatings.

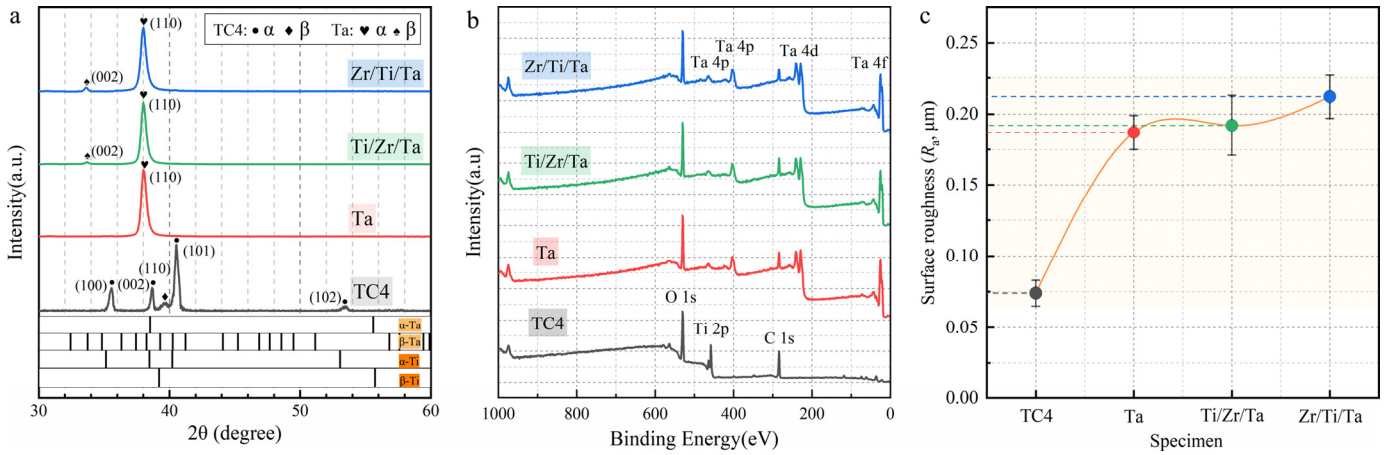


Figure 1. Basic characteristics of the sample surface. (**a**) XRD patterns of TC4 and the different coating samples with insert standard peak position of pure Ti and Ta, (**b**) XPS spectra of TC4 and the different coating samples, and (**c**) surface roughness of the samples without and with coatings.

XPS was applied to obtain more information about the surface composition and state of chemical bonding of the experimental samples (Figure 1b). Surface composition and chemical states are ones of the important factors affecting surface properties, especially corrosion behavior and electrochemical corrosion performance. Since Ti, Zr and Ta as well as their alloys are passivated metals, their corrosion resistance strongly depends on the passivation film generated on the surface. For all samples, the peak with the binding energy of around 530 eV (O 1s) was attributed to a metal oxide. The Ti 2p XPS spectra showed that the main component of the passivation film on the TC4 substrate was TiO_2. Three groups of peaks at 20–28 eV (Ta 4f and Ta), 220–240 eV (Ta 4d) and around 401 eV (Ta 4p) were detected in the coating samples, which corresponded to Ta_2O_5, TaO_2, TaO and metallic Ta. It is noteworthy that the presence of high valence oxides decreases the corrosion rate and stabilizes the passivation film of the alloy [23]. Our previous work [13] has discussed

the surface chemical states and the effect of high-valence oxide Ta_2O_5 on the corrosion resistance of coating samples. In this study, the composition of the coating samples was the same, and all of them had the Ta outermost layer and possessed high purity, which resulted in similar XPS spectra. This consistency of chemical states is more conducive to the investigation of the effect of structural differences on the surface properties of coatings.

The surface roughness (R_a) of the TC4 substrate and various coating samples is presented in Figure 1c. The parameter R_a of polished TC4 substrate was controlled below 0.1 μm, and after coating preparation, the R_a values of the coated samples were increased to 0.2 μm. The basic characteristic parameters of the different samples are listed in Table 1. From the R_a results, the variation of surface roughness is mainly affected by the nucleation and growth of each layer. A common growth mode of polycrystalline films is the Volmer–Weber mode [24], which comprises three stages: (i) island nucleation and growth, (ii) island coalescence, and (iii) post-coalescence film thickening. After the final stage, a continuous film is growing, and the surface will have a tendency to form a grain structure leading to an increased surface undulation. In addition to this, the electrical parameters during deposition, the composition and structure of coatings can also affect the R_a of the coating. Under the joint action of these factors, the surface roughness increased.

Table 1. Basic characteristic parameters of different samples.

Samples	TC4	Ta	Ti/Zr/Ta		Zr/Ti/Ta	
Surface roughness (R_a/μm)	0.074 ± 0.009	0.187 ± 0.012	0.192 ± 0.021		0.212 ± 0.015	
Coating thickness (μm)	\	3.18	Total	2.87	Total	2.93
			Ti	1.03	Zr	0.82
			Zr	0.84	Ti	1.11
			Ta	1.00	Ta	1.00

Fracture cross-sectional SEM images of the coatings are shown in the Figure 2, and the results for the coating thickness are listed in Table 1. According to the images, all the outermost layers of the samples were Ta, and the total coating thickness of each coating was about 3 μm. The multilayer Ti/Zr/Ta and Zr/Ti/Ta coatings contained Ti, Zr and Ta layers with an average thickness of 1 μm, respectively. The original intention of the sample preparation is that each coating has the same thickness. However, in order to ensure the continuity of the target material deposition, each subsequent layer was sputtered in advance manually, which was mainly affected by the human factors. Moreover, the deposition rates of the three metals were different. To achieve the roughly the same thickness of each layer, the deposition time of layers also varied. A slight deviation in time or deposition rate would have led to different thicknesses of the constituent layers within the margin of error. In the right side of the figures, a columnar structure inside of the monolayer coating was normally coarser than that in the multilayer coatings, which could be attributed to the long duration of sputtering. The extended deposition time, in turn, caused the accumulation of more kinetic energy and the increase of the temperature near the coating, triggering the formation of coarser columnar structures [8,25]. In addition to this, the interlayer interface of the multilayer structure would also have effectively hindered the growth of the columnar grains. In multilayer coatings, the growth of some columnar grains stops at the layer interfaces, while others start growing, as the layer interfaces provide more opportunities for the nucleation of new crystal grains. These processes result in a refinement of crystal grains, although there were columnar structures crossing the interlayer interface by reason of the advance deposition of next coating material. The columnar crystals were still difficult to grow into the third layer (i.e., through the entire thickness direction) due to the blocking effect of the phase interfaces and grain boundaries. Therefore, the coarser and longer columnar structures of the monolayer Ta coating were observed after the continuous single element deposition.

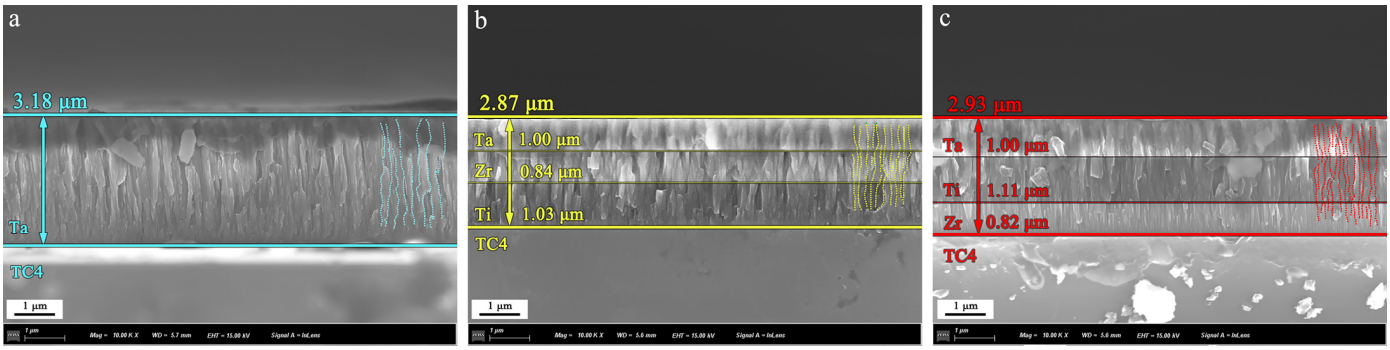


Figure 2. Cross-sectional morphology of the (**a**) Ta, (**b**) Ti/Zr/Ta and (**c**) Zr/Ti/Ta coatings.

Adhesion of the coating is one of the key factors in the service life of coating products [8]. In this study, the scratch method was applied to evaluate the critical adhesion loads of the monolayer Ta and multilayer Ti/Zr/Ta and Zr/Ti/Ta coatings. As the indentation load increased, the fracture, delamination, fragmentation and even peeling off from the substrate occurred along the direction of the scratch. In this paper, the critical load can be used to characterize the bonding force between the coating and substrate. To evaluate the adhesion of coatings, the minimum critical adhesion load was determined at the moment when the coating first peeled off or the TC4 substrate was first exposed during the scratch test. Figure 3 depicts the nano-scratch morphologies of the coating samples, and the locations of the matrix first exposed are also marked.

The critical adhesion load of the monolayer Ta was ~265 mN, which was significantly higher than that of the multilayer Ti/Zr/Ta (~183 mN) and Zr/Ti/Ta (~178 mN). As shown in the figure, the scratch track of Ta was smooth and narrow before the first fracture. As the load increased to ~265 mN, the coating cracked and the TC4 substrate was exposed, showing a clear and uniform scratch track. The enlarged images (Figure 3b–d) show the locations of the matrix first exposed (i.e., critical adhesion load) of each coating sample as determined by SEM after carrying out the scratch. It can be found that the scratch of sample Ta was relatively smooth and clear, with only a small piece of Ta coating peeling off. However, the coating started to be broken when the critical adhesion load was reached. Coating cracks spread rapidly to both sides of the scratch, where crushed and broken coating fragments accumulated. Sparse cracks propagated in the direction perpendicular to the scratch and were parallel to each other; meanwhile, the crack propagation depth was shallow, and the coating fragmentation area was small as well. The morphologies of the scratch track of the Ti/Zr/Ta and Zr/Ti/Ta coatings were similar, indicating a linear increase in the width of the scratch with increasing load. At the location of first fracture (Figure 3c,d), large ares of delamination of the coatings occurred, resulting in the substrate exposure. Delamination and failure of the Zr/Ti/Ta coating was the most obvious, exhibiting a large area of brittle spalling on both sides of the scratch. This brittle fracture mechanism prevails with the formation of transverse cracks [26]. Consequently, the adhesion of multilayer Ti/Zr/Ta and Zr/Ti/Ta coatings was weaker than that of single-layer Ta coating, mainly because the chemical bonding, lattice misfit and van der Waals forces between the interlayer and the layer-substrate had the more serious effects on the interlayer synergies.

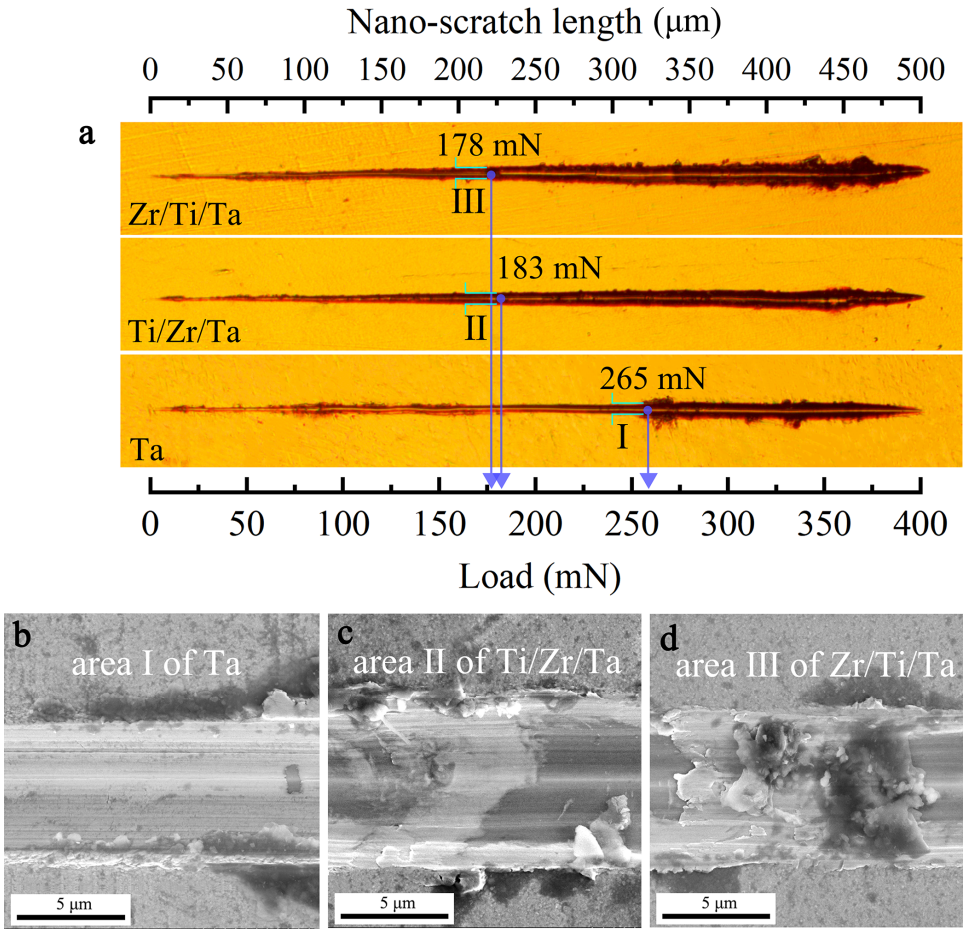


Figure 3. The scratch graphs of monolayer Ta coating and multilayer Ti/Zr/Ta and Zr/Ti/Ta coatings. (**a**) Overall scratch graphs and (**b**–**d**) representative areas of the matrix first exposed on the samples Ta, Ti/Zr/Ta and Zr/Ti/Ta.

3.2. Tribological Properties

Friction and wear tests of the current samples were carried out in ball-on-disk mode at room temperature in the SBF solution and atmospheric environment, respectively. Figure 4 shows the friction coefficient (COF) and wear rate curves of the samples in the two test environments. In the SBF solution environment (Figure 4a), the fluctuation of the COF value under the influence of liquid flow and resistance was obvious. The variation trend of COF was similar for all samples: it first increased in the initial stage, then decreased in the running-in state, and finally leveled off in the steady wear state. The average COFs of the TC4 substrate, Ta, Ti/Zr/Ta and Zr/Ti/Ta in the solution environment were 0.52, 0.33, 0.39 and 0.46, respectively. In the atmospheric environment (Figure 4b), the COF values changed to a slight extent. Meanwhile, those of the coatings showed a tendency of gradual increase and stabilization, while the COF value of the TC4 substrate experienced a large increase and decrease in the breaking-in period (500–1500 laps), indicating the distinguishable wear behavior. The average COFs of the TC4 substrate, Ta, Ti/Zr/Ta and Zr/Ti/Ta in the atmospheric environment were 0.67, 0.52, 0.59 and 0.60, respectively. The overall wear in the same environment varied in descending order as follows: Ta → Ti/Zr/Ta → Zr/Ti/Ta → TC4, which was also confirmed by the wear rate (WR) results (Figure 4c). However, the WRs of the same sample greatly varied under different experimental conditions; in addition to this, both the COF and WR were significantly higher in the atmospheric environment than in the SBF solution.

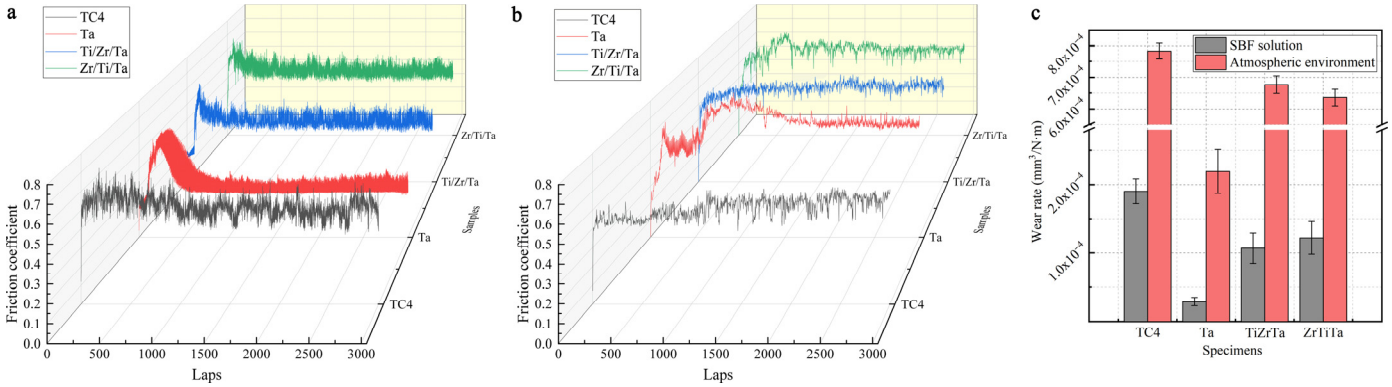


Figure 4. The friction coefficient of the TC4 substrate and the different coating samples at room temperature in (**a**) SBF solution and (**b**) atmospheric environment, and (**c**) wear rate of the TC4 substrate and the different coating samples in two experimental environments.

Figure 5 displays the wear track morphologies of the experimental samples in the SBF solution environment under different magnifications. Thanks to different imaging tools and contrast degrees, SEM and OM can bring out more detail about morphological features for comparative analysis. In this study, the laser scanning confocal microscope was used to characterize the wear tracks in the coatings, and the corresponding 2D-profile morphologies and 3D images are shown in Figure 6. According to Figure 5a–c, the typical deep and wide wear tracks as well as the parallel grooves with black debris have appeared in the worn TC4 substrate. Given the 2D and 3D morphological profiles in Figure 6a–c, the width and depth of the track reached ~568.8 μm and ~3.8 μm, respectively, revealing the most severe wear among the coatings under consideration. On the contrary, the monolayer Ta coating had the minimum track width (~263.9 μm, Figure 5d) and the shallowest wear track (~263.9 μm, Figure 6d–f). As seen from the zone I in Figure 5f, the abrasion of Ta was mainly concentrated on one side of the wear track. Severe friction positions displayed the furrow morphology, indicating the abrasive wear; meanwhile, the smooth glazed layers appeared on the friction surface. Moreover, as shown in Figures 5g–l and 6g–l, the multilayer Ti/Zr/Ta and Zr/Ti/Ta coatings exhibited similar depth and width of the tracks, and their wear resistance was better than that of the TC4 substrate. However, the wear mechanism of Ti/Zr/Ta and Zr/Ti/Ta is quite different from that of TC4 substrate. Except for the wear debris and grooves, the coating fragmentation and delamination existed at the edge of the wear track, as shown in zone II (Figure 5i) and zone III (Figure 5l). Under the scouring action of the solution, few fragments adhered to the unpeeled coating. At the edge of the abrasion track, the delamination was obvious, and the ruptured edge of the coating was clear.

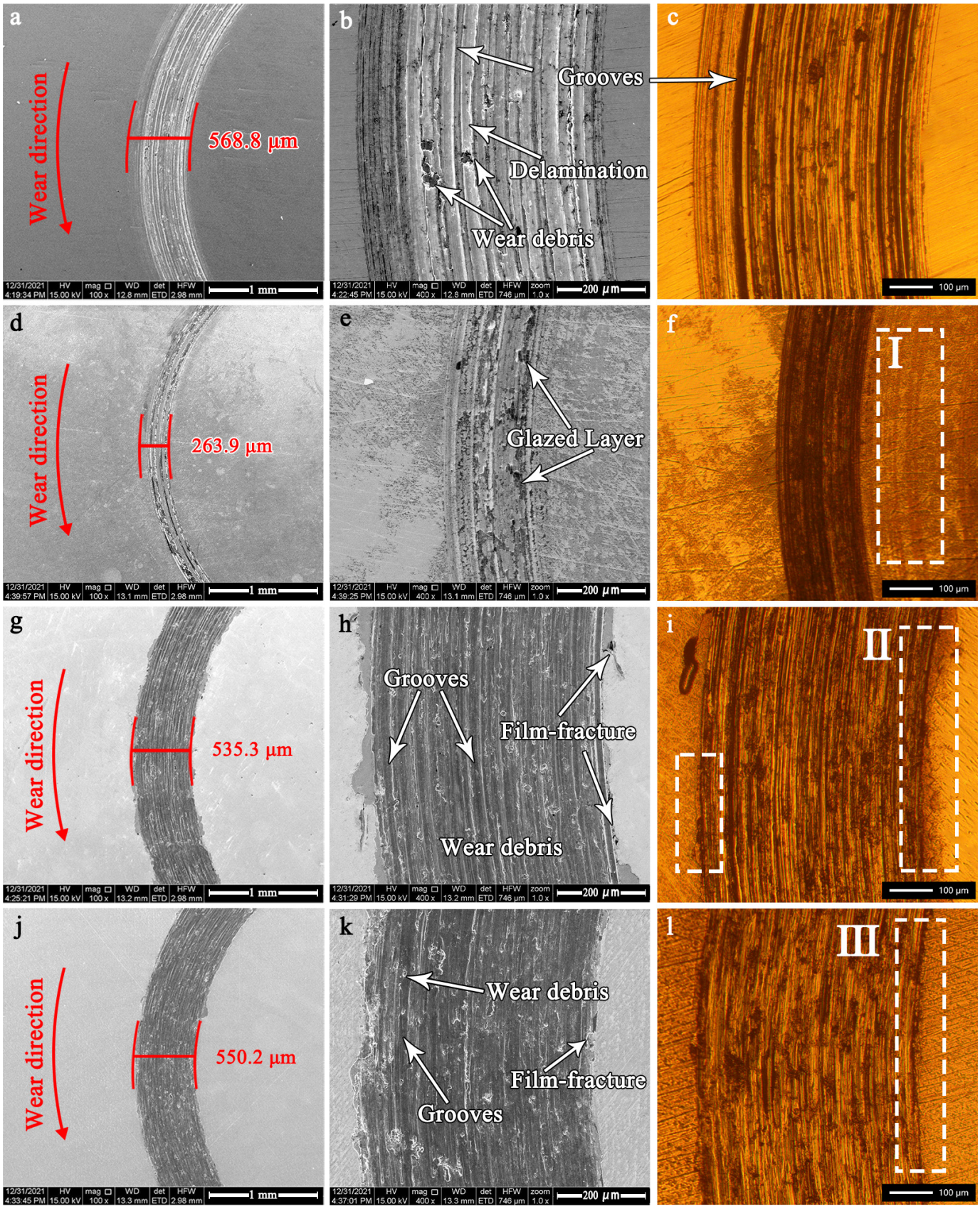


Figure 5. The OM and SEM wear track morphologies under SBF solution environment of (**a**–**c**) the TC4 substrate, (**d**–**f**) the Ta, (**g**–**i**) the Ti/Zr/Ta, and (**j**–**l**) the Zr/Ti/Ta. (I–III) are the zones inside and outside the wear track of the Ta, Ti/Zr/Ta, and Zr/Ti/Ta, respectively.

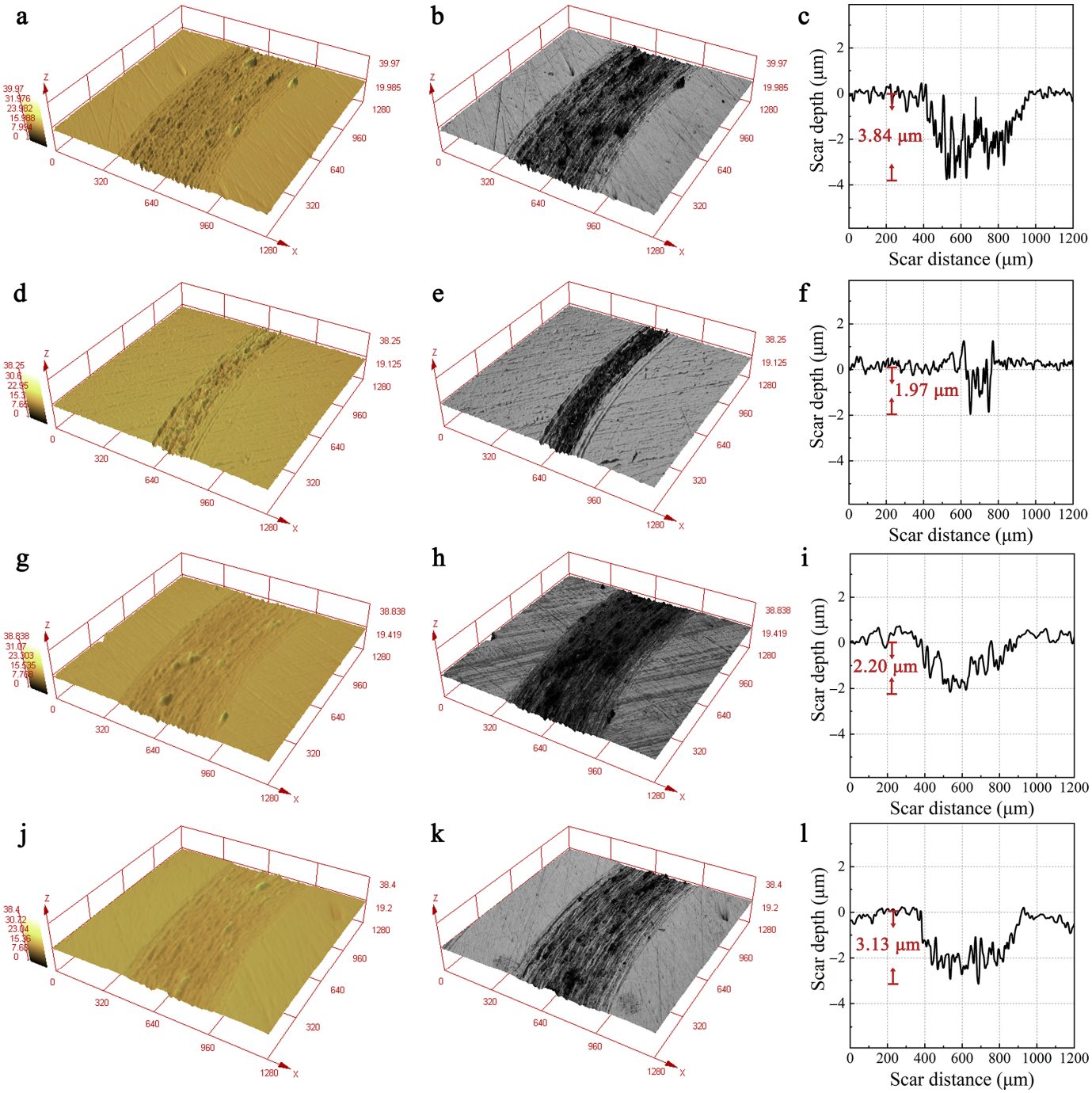


Figure 6. 3D morphologies and 2D profiles of wear track under SBF solution environment of (**a**–**c**) the TC4 substrate, (**d**–**f**) the Ta, (**g**–**i**) the Ti/Zr/Ta, and (**j**–**l**) the Zr/Ti/Ta.

Figures 7 and 8 depict the wear track morphologies along with the 2D and 3D morphology profiles generated in the atmospheric environment. According to the width and depth of the wear track, the antiwear performance of Ta was superior to that of Ti/Zr/Ta, Zr/Ti/Ta and TC4 substrate. The overall wear of all samples was consistent with the results obtained in the SBF solution. Under the double action of thermal and oxidation influences, the furrow morphologies and tongue-shaped wedges appeared on the wear track of TC4 substrate, demonstrating that the wear behaviors were affected by mechanisms of adhesive wear and abrasive wear simultaneously (Figure 7c). After the preparation of the monolayer Ta coating, the edge of the wear track was blurred, and the track surface was smeared with black debris which might be the product of wear transferred from the counterpart

ball. This appeared as the island bulge in the middle of the track, as seen from the color contour plot in Figure 7d. In Figure 7d, the inside (zone II) and outside (zone I) of the wear track also exhibited different wear conditions. The gradually wearing Ta coatings and glazed layers with adhering debris can be observed in zone I and zone II, respectively. This nonuniformity of the unilateral compressive state might have been caused by the errors associated with the sample placement. Under the dry friction condition, the multilayer Ti/Zr/Ta and Zr/Ti/Ta coatings still displayed a similar wear resistance to that of TC4 substrate. Compared with the solution environment, the area of the coating at the edge of the wear track was larger (see zone III in Figure 7h and zone IV in Figure 7k), and the broken outermost layer still adhered to the substrate after the wear test. Furthermore, by comparing Figures 6 and 8, a round valley-like morphology was found in the wear scar of the multilayer samples after dry friction; besides, the furrows were clearer and the degree of wear increased. Although the step profile was blurred at the edge of the wear track in the 2D profiles, it was still observed due to the high detection accuracy and large signal fluctuations, providing evidence for coatings peeling off. The wear parameters of all the experimental samples are listed in Table 2 for reference analysis. Considering the wear morphologies and wear parameters, the anti-wear performance of the same sample in the SBF solution environment was much stronger than that in the atmosphere environment. Moreover, the anti-wear performance of the Ta coating in the same experimental environment exceeded that of the multilayer samples and TC4 substrate.

Table 2. Wear parameters of different specimens according to the morphology observation and confocal laser analysis.

Experimental Environment	**SBF Solution Environment**				**Atmospheric Environment**			
Samples	**TC4**	**Ta**	**Ti/Zr/Ta**	**Zr/Ti/Ta**	**TC4**	**Ta**	**Ti/Zr/Ta**	**Zr/Ti/Ta**
Average COF	0.52	0.33	0.39	0.46	0.67	0.52	0.59	0.60
WR ($mm^3/N{\cdot}m$) ($\times 10^{-4}$)	1.90	0.29	1.07	1.22	7.83	2.19	6.77	6.36
Width of wear track (μm)	568.8	263.9	535.3	550.2	834.6	318.5	812.6	813.9
Depth of wear track (μm)	3.8	2.0	2.2	3.1	13.7	10.2	11.3	11.1

3.3. Abrasion Mechanisms

Under two different test environments, laminar tearing appeared on the wear track of the TC4 substrate, and the wear mechanism was dominated by plastic deformation and adhesive wear. Given the fact that the shear stress component of the normal force was greater than the shear strength of the friction materials, shear deformation occurred, and laminar tearing patterns formed [27]. However, the GCr15 ball was harder than the TC4 substrate, and the friction contact surface of the ball was gradually roughened with the sliding wear, resulting in abrasive wear on the soft surface of TC4 substrate. Adhesive wear and abrasive wear occurred simultaneously on the monolayer Ta coating. Unlike the TC4 substrate, the adhesive wear of the monolayer Ta was due to the increase of surface hardness after the coating deposition, which made the GCr15 ball become a soft friction pair, and the increase of surface roughness. Under the stress state, the two friction surfaces are affected by the effect of solid bonding, and the adhesive wear is generated by the adhesion of these surfaces at the micro-convex position [28]. For all the coating samples in the atmospheric environment, there were severe furrows on the wear track, indicating that the wear mechanism of abrasive wear was more significant. Figure 9 displays the schematic illustration of macroscopic wear mechanisms within the coatings in different environments.

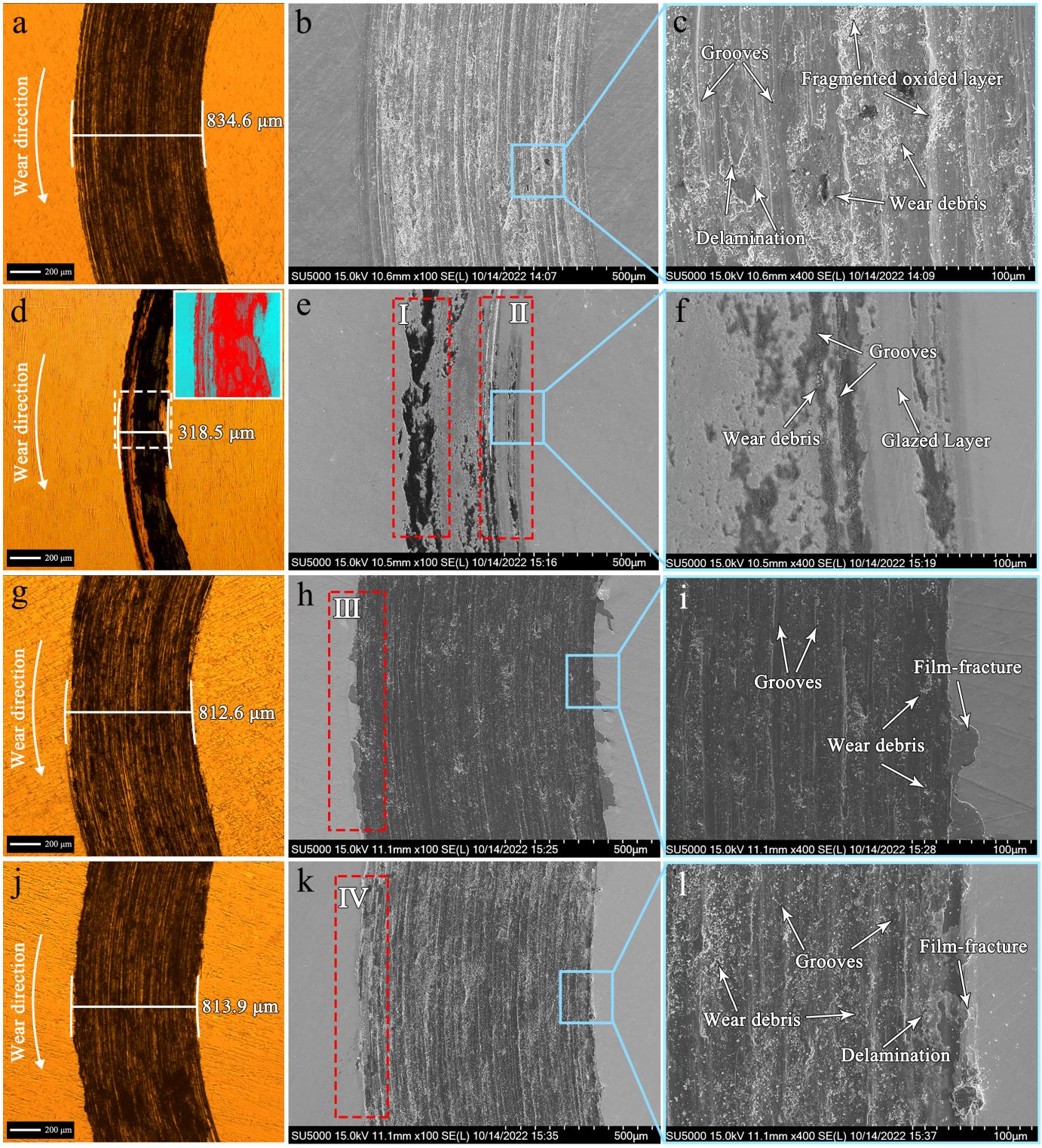


Figure 7. The OM and SEM wear track morphologies in atmospheric environment of (**a**–**c**) the TC4 substrate, (**d**–**f**) the Ta, (**g**–**i**) the Ti/Zr/Ta, and (**j**–**l**) the Zr/Ti/Ta. (I) and (II) are the zones inside and outside the wear track of the Ta, (III) and (IV) are the zones outside the wear track of the Ti/Zr/Ta and Zr/Ti/Ta, respectively.

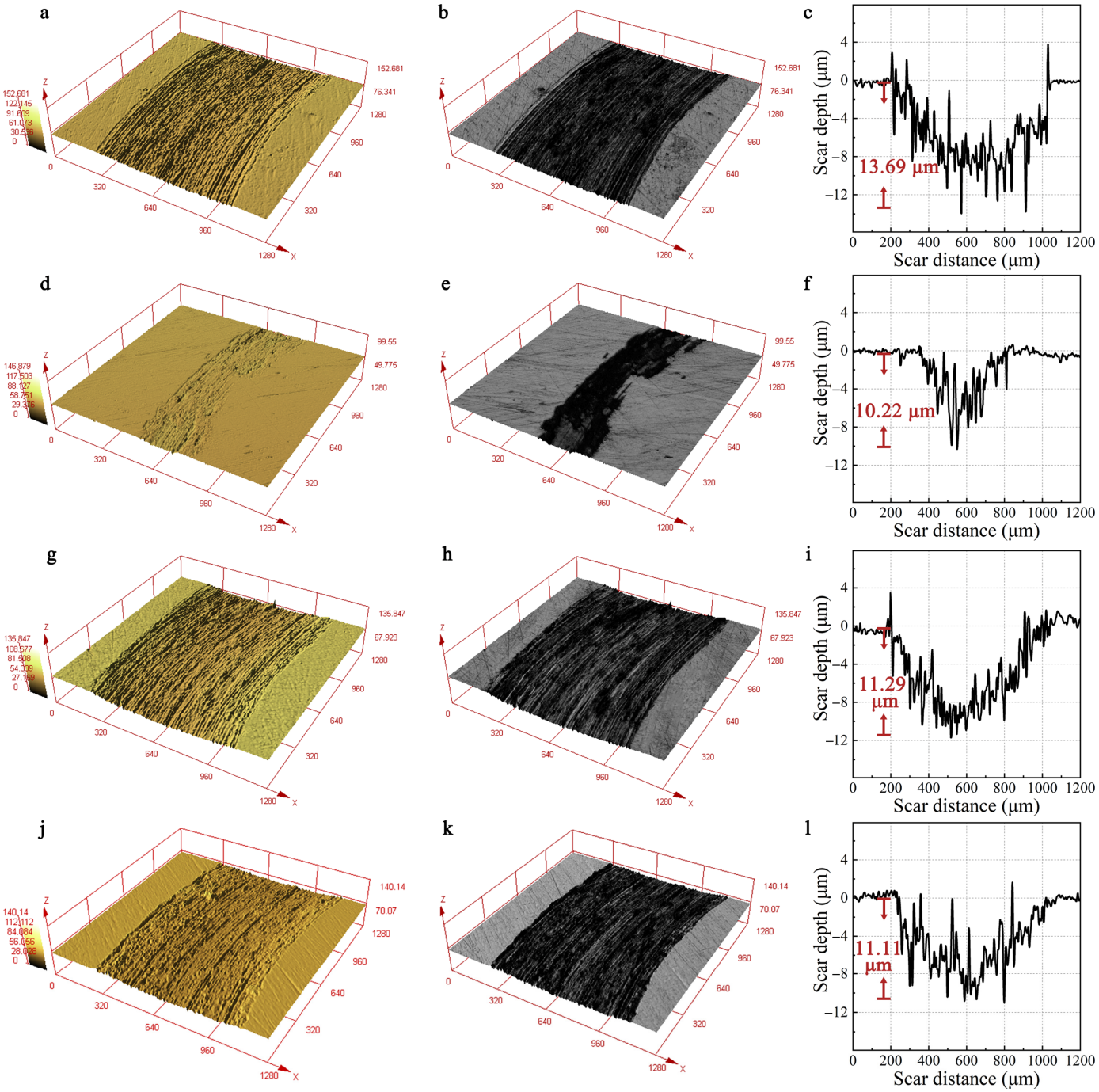


Figure 8. 3D morphologies and 2D profiles of wear track in atmospheric environment of (**a**–**c**) the TC4 substrate, (**d**–**f**) the Ta, (**g**–**i**) the Ti/Zr/Ta, and (**j**–**l**) the Zr/Ti/Ta.

According to the above results, the samples in the SBF solution demonstrated lower COF and WR values as well as a shallower and narrower wear track than those in the dry condition, suggesting the remarkable dependence of the TC4 substrate and coatings on the wear environment. Generally, lubrication is conducive to the protection of the friction materials, and the solution along with the electrolyte perform as lubricants during the sliding contact [19,29,30]. In addition, the friction pair slides to drive the flow of the solution in the environment. Under the scouring action of the solution, the debris generated in the last lap will be washed away or continuously suspended in the liquid, which reduces the wear caused by the abrasive debris and plays a friction-decreasing role. Although there were abundant ions in the solution, their erosion effect was not significant due to the short

tribological wear period, and no obvious corrosion wear was been detected. The macroscopic friction and wear mechanisms in the SBF solution environment are shown in Figure 9a.

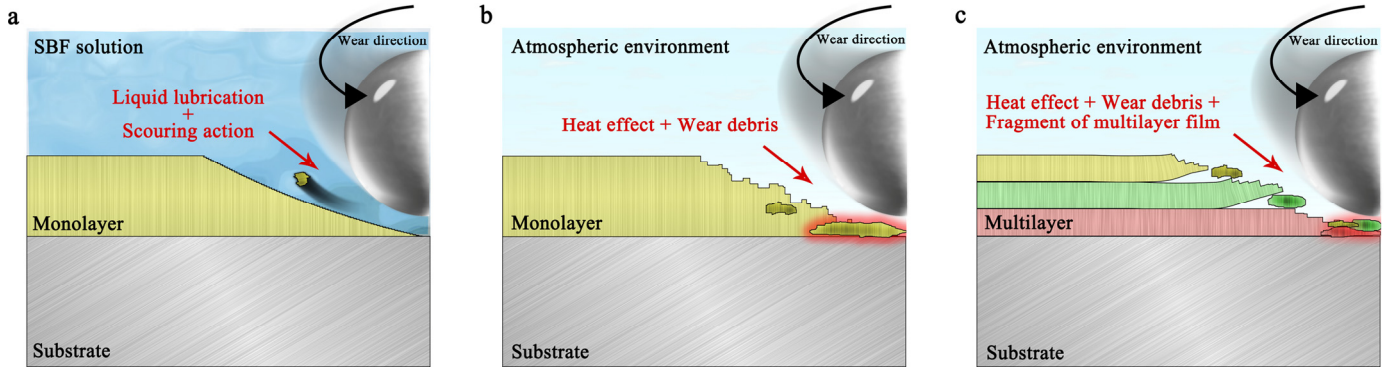


Figure 9. Schematic illustration of macroscopic wear mechanisms of (**a**) the monolayer Ta in SBF solution environment, (**b**) the monolayer Ta in atmospheric environment and (**c**) the multilayer coating in atmospheric environment.

In the same experimental environment, the wear parameters of multilayer Ti/Zr/Ta and Zr/Ti/Ta coatings were similar, being slightly better than that of TC4 substrate and lower than that of monolayer Ta. The wear mechanisms of monolayer and multilayer coatings were quite different under the dry condition, wherein the wear patterns were clearer and convenient for the analysis. It can be seen from Figures 7f and 10a that the wear damage of monolayer Ta at the edge of the wear track has been caused by a gradual wear process. However, the edges of the wear tracks in the multilayer Ti/Zr/Ta and Zr/Ti/Ta coatings (Figure 7i or Figure 10b) were well-defined and accompanied by the coating damage, indicating that the brittle failure mechanism played an important role in the abrasive wear. This is because of poor cohesion and adhesion caused by the composition of each layer, structure of the coatings, interface structure and residual stress in the coatings [31–33]. It is noteworthy that distinguishing between the layer-to-layer adhesion and the coating-to-substrate adhesion is a challenge. Good adhesion strength between the coating and the underlying substrate is a key requirement for wear-resistant protective coatings [32]. The fracture behaviors were also presumably related to the hierarchical design [33], in this study, the discontinuous columnar structure created by hierarchical deposition further reduced the adhesion of the multilayer coating. Furthermore, the coating became thinner and the cyclic stress imposed on the substrate/coating interface increased under the progressive wear. Depending on the adhesion between the coating and the substrate, a rapid decohesion of the film below a critical coating thickness (or a threshold stress value) will be activated, leading to a failure of the whole coating [28]. Each layer in the multilayer coating was relatively thin, resulting in a critical coating thickness, that is, the layer-by-layer peeling off was easily induced. In general, the metastable tetragonal β phase of Ta is harder and more brittle than the α phase [34,35]. The existence of β phase in the outmost layer of the multilayer coating promoted the brittle fracture and the formation of a neat cleavage plane. Then, the fragments of the exfoliation layer together with the wear debris aggravated the abrasive effect and wear rate under the influence of friction heat effects (Figure 9b,c).

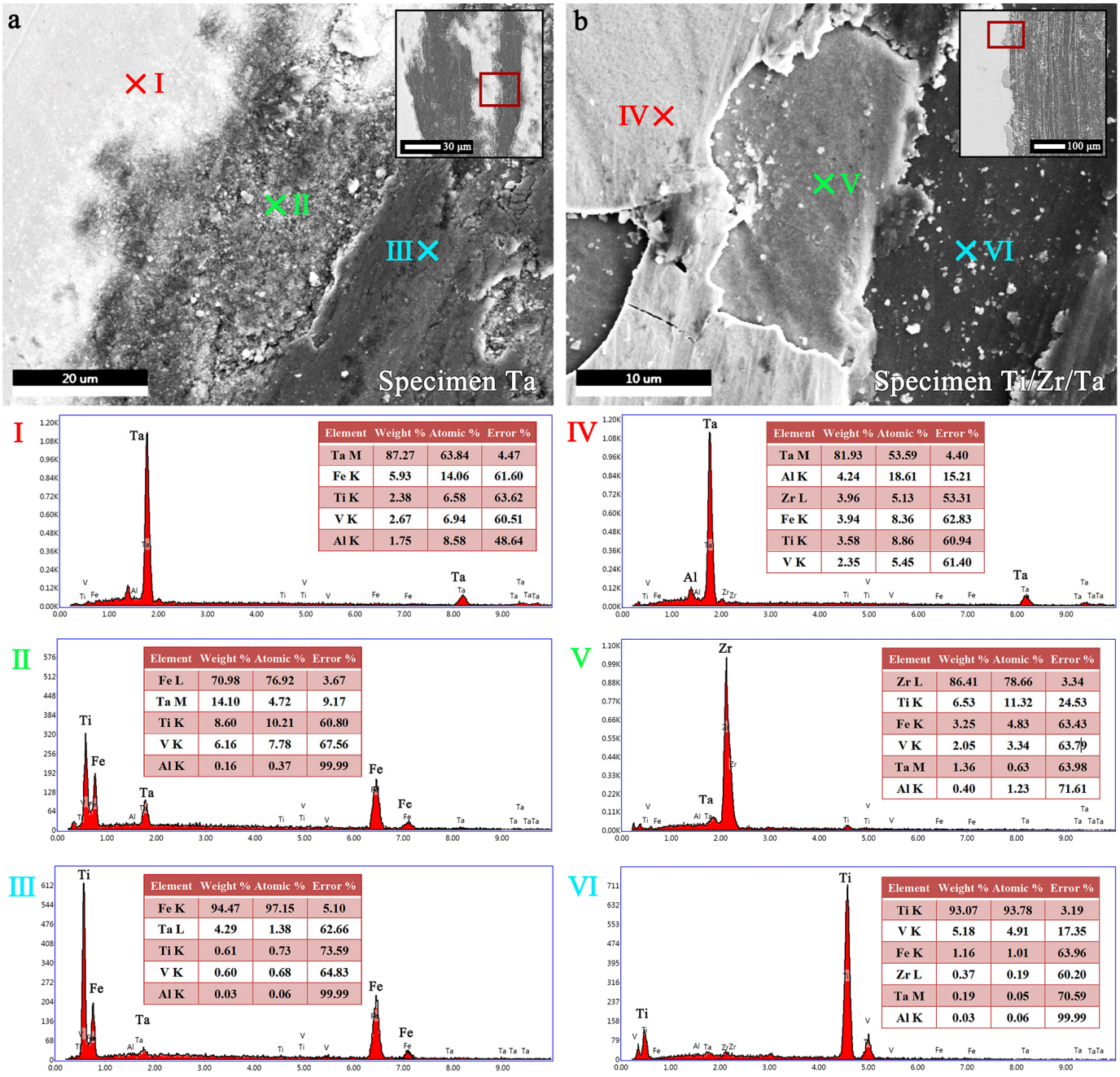


Figure 10. EDS results at typical wear locations of (**a**) the monolayer Ta and (**b**) the multilayer Ti/Zr/Ta coatings after dry friction test. (I–III) are the spots in the wear characteristic zones of the Ta, and (IV–VI) are the spots in the wear characteristic zones of the Ti/Zr/Ta.

The reason for high durability of the monolayer Ta coating was that, in addition to the excellent coating structure and coating-substrate adhesion, it had the large thickness and exhibited a certain solid lubrication and wear-reducing effect. As a sufficiently thick coating prevents the friction pair from reaching the substrate, it has caused the wear to occur in the Ta coating. Thus, the possibility of excessive adhesion and plastic deformation was reduced [29]. Ta is a typical passivated metal which can be covered by a thin oxide layer under normal temperature and pressure, and the above XPS results could confirm the existence of Ta_2O_5 on the coating surface. Qin et al. [36] have explained the mechanisms for good lubrication of the Ta oxide from three aspects: (i) formation of Ta oxide reduces the shear stress on tribofilm, (ii) low wear conditions, and (iii) continuous formation of

lubricating wear products on the contact surface. In this study, as the friction process proceeded, steady Ta oxide layers formed on the worn surface of the Ta coating under the higher friction contact temperature, thereby leading to larger areas of oxide films formation on the worn surface. These oxide films, serving as efficient solid lubricant [36,37], could reduce adhesion between the coating and the GCr15 steel ball, thus decreasing the COF. The result of COF reduction can be confirmed by Figure 4a,b. Hence, the monolayer Ta coating provided sufficient thickness for the formation of oxides and continuous wear.

Figure 10 depicts the EDS spot scanning results on the monolayer Ta and multilayer Ti/Zr/Ta surfaces after wear testing, which further confirmed the occurrence of the above wear behaviors. When the factors of the signal drift, spot size, analysis method (spot or area analysis), excitation volume, shading, time of acquisition, etc., are taken into account in the precise detection process, the margin of error represents the reliability of EDS data.

It is generally known that the error on the main element is less than 10%, the error on the element with the content of 1 wt.%–3 wt.% is less than 30%, and the error on the element with the content lower than 1 wt.% is below 50%. So, when the error rate exceeds 50%, the data will be deemed invalid [38]. In this study, conventional methods were used in EDS detection, which was mainly applied for qualitative analysis, and the measurement accuracy was much lower than that of the precise detection. All possible elements were selected in the program, and the data presented in Figure 10 were the original data, among which the EDS results with high error rate and low content could be judged to be unreliable. The reliable element content results could be used to determine the dominant elements in the detected area, and these results could be also used to confirm the wear and layer peeling of the coatings. For the worn monolayer Ta coating, spots labeled I, II and III are the locations of mild wear, severe wear and transferred material, respectively. The result at spot I revealed that the main element was Ta, and there was a small amount of coating wear at this position. As the wear evolved, Fe and a small amount of Ta were detected (spot II). Abundant iron was detected where the substrate material was fully exposed (spot III), which was transferred from the ball to the sample disk as a result of adhesive wear. In the top of Figure 10a, a mixture of incomplete peeling coating particles and their oxides was also observed, which was important evidence of abrasive wear. For the worn multilayer Ti/Zr/Ta coating, the EDS spot scanning was conducted at the edge of the wear track. No sliding wear track was observed at this position, but the coating was splintered and peeled off, suggesting the mechanism of brittle fracture. The bottom right corner in Figure 10b shows the plastic deformation morphology of the substrate undergoing wear after the coating failure. The results at spots IV, V and VI revealed the presence of Ta, Zr and Ti, respectively, which were consistent with the coating structure design. Some fragments were also observed on the surface of each layer. Therefore, the findings of this study further explained the differences in wear resistance and wear mechanisms between the monolayer and multilayer coatings.

4. Conclusions

In this work, the monolayer Ta and multilayer Ti/Zr/Ta and Zr/Ti/Ta coatings were prepared on TC4 substrates by magnetron sputtering. The microstructure, surface composition, tribological properties and wear mechanisms of the coatings were studied. Based on the results, the conclusions can be drawn as follows.

The XRD data revealed that the TC4 substrate consisted of the typical α + β dual phase, whereas only the stable bcc α-Ta phase was detected in the monolayer Ta coating, and the stable bcc α-Ta phase together with metastable tetragonal β-Ta inclusions coexisted in multilayered Ti/Zr/Ta and Zr/Ti/Ta coatings. The XPS spectra showed that the main component on the surface of the TC4 substrate was TiO_2, and those on the coating samples were the high-valence Ta_2O_5 oxides accompanied by a small amount of TaO_2, TaO and metallic Ta.

The R_a increased from below 0.1 μm for the uncoated substrate to around 0.2 μm after the coating deposition. Coating growth was followed Volmer–Weber mode, and the

tendency of the surface to form grain structure resulted in increased R_a. The total coating thickness of each coating sample was about 3 μm. The monolayer Ta coating exhibited the continuous and coarse columnar structure, while that of the multilayer coatings was discontinuous and fine.

After the scratch tests, only a small piece of Ta coating peeled off on the monolayer Ta; however, the substrates were completely exposed on multilayer Ti/Zr/Ta and Zr/Ti/Ta coatings at the locations of the critical adhesion loads. The first fracture of the monolayer Ta and multilayer Ti/Zr/Ta and Zr/Ti/Ta coatings occurred when the load reached 265, 183 and 178 mN, respectively, indicating that the monolayer Ta coating had stronger adhesion than that of multilayer coatings.

In both the SBF solution and atmospheric environments, the results on the COFs, WRs, depth and width of the wear track of the monolayer Ta coating were the best among the all studied samples. The corresponding values for Ti/Zr/Ta and Zr/Ti/Ta multilayer coatings were similar but slightly exceeded that of the TC4 substrate. Thanks to the liquid lubrication and scouring action, the wear parameters of all the studied samples in the solution environment were significantly better than those under the dry condition. Moreover, the wear mechanism of the monolayer Ta coating was different from that of multilayer coatings. The monolayer Ta coating possessed the best wear resistance, which was attributed to its dense coating structure, good adhesion to the substrate, sufficient Ta coating thickness, and solid lubrication effect of the oxide. For good lubricating properties, the friction heat caused continuous production of Ta oxide, and the Ta oxides reduced adhesion between the friction pairs effectively decreasing the COF. Furthermore, the monolayer Ta coating provided sufficient thickness for oxide formation in continuous wear. The main wear mechanisms of the monolayer Ta were abrasive wear and adhesive wear. The worn surface of the monolayer Ta was relatively smooth with a small amount of debris hindering the initiation and propagation of cracks. In contrast, the anti-wear properties of multilayer coatings were weak owing to the poor layer-to-layer and coating-to-substrate adhesion as well as the discontinuous columnar structure. Therefore, a mixture of abrasive wear and brittle fracture was identified as the predominant wear mechanism of the multilayer coatings, and the considerable wear debris produced in the friction process resulted in a increase of wear loss.

The WRs of the monolayer Ta coating were 0.29×10^{-4} and 2.19×10^{-4} $mm^3/N{\cdot}m$ in the SBF solution and atmospheric environments, respectively. Compared with the substrate and the multilayer coatings, the wear resistance of the monolayer Ta coating is improved by 84% and 72%–76% under solution conditions, 72% and 66%–68% under dry conditions, respectively, showing it to be a promising material for biomedical applications.

Author Contributions: Conceptualization and supervision, Y.Y.; methodology, writing and editing, S.L.; formal analysis, W.Q.; resources and project administration, F.W.; data curation, Y.X.; visualization and review, C.X.; software and validation, S.D. All authors have read and agreed to the published version of the manuscript.

Funding: This work was supported by Major Science and Technology Project of Henan Province (Grant No. 221100210500) and China Postdoctoral Science Foundation (Grant No. 2021M700490).

Institutional Review Board Statement: Not applicable.

Informed Consent Statement: Not applicable.

Data Availability Statement: The raw/processed data required to reproduce these findings cannot be shared at this time as the data also form part of an ongoing study.

Acknowledgments: Special thanks go to Sen Yang for experimental assistance.

Conflicts of Interest: The authors declare no conflict of interest.

References

1. Kunčická, L.; Kocich, R.; Lowe, T.C. Advances in metals and alloys for joint replacement. *Prog. Mater. Sci.* **2017**, *88*, 232–280.
2. Wauthle, R.; Van Der Stok, J.; Yavari, S.A.; Van Humbeeck, J.; Kruth, J.-P.; Zadpoor, A.A.; Weinans, H.; Mulier, M.J. Additively manufactured porous tantalum implants. *Acta Biomater.* **2015**, *14*, 217–225. [CrossRef] [PubMed]
3. Bonnheim, N.B.; Van Citters, D.W.; Ries, M.D.; Pruitt, L.A. Oxidized zirconium components maintain a smooth articular surface except following hip dislocation. *J. Arthroplasty* **2021**, *36*, 1437–1444. [CrossRef] [PubMed]
4. Jain, S.; Parashar, V. Analytical review on the biocompatibility of surface-treated Ti-alloys for joint replacement applications. *Expert. Rev. Med. Devic.* **2022**, *19*, 699–716. [CrossRef] [PubMed]
5. Cabrera-Domínguez, J.J.; Castellanos-Cosano, L.; Torres-Lagares, D.; Pérez-Fierro, M.; Machuca-Portillo, G. Clinical performance of titanium-zirconium implants with a hydrophilic surface in patients with controlled type 2 diabetes mellitus: 2-year results from a prospective case-control clinical study. *Clin. Oral. Invest.* **2020**, *24*, 2477–2486. [CrossRef]
6. Ionita, D.; Pirvu, C.; Stoian, A.B.; Demetrescu, I. The trends of TiZr alloy research as a viable alternative for Ti and Ti16 Zr roxolid dental implants. *Coatings* **2020**, *10*, 422. [CrossRef]
7. Elias, L.; Schneider, S.; Schneider, S.; Silva, H.; Malvisi, F. Microstructural and mechanical characterization of biomedical Ti–Nb–Zr (–Ta) alloys. *Mat. Sci. Eng. A-Struct* **2006**, *432*, 108–112. [CrossRef]
8. Su, Y.; Huang, W.; Zhang, T.; Shi, C.; Hu, R.; Wang, Z.; Cai, L. Tribological properties and microstructure of monolayer and multilayer Ta coatings prepared by magnetron sputtering. *Vacuum* **2021**, *189*, 110250. [CrossRef]
9. Wang, X.; Ning, B.; Pei, X. Tantalum and its derivatives in orthopedic and dental implants: Osteogenesis and antibacterial properties. *Colloid. Surface. B* **2021**, *208*, 112055.
10. Beline, T.; da Silva, J.H.; Matos, A.O.; Neto, N.F.A.; de Almeida, A.B.; Júnior, F.H.N.; Leite, D.M.; Rangel, E.C.; Barao, V.A. Tailoring the synthesis of tantalum-based thin films for biomedical application: Characterization and biological response. *Mat. Sci. Eng. C-Mater* **2019**, *101*, 111–119. [CrossRef]
11. Liu, Y.; Bao, C.; Wismeijer, D.; Wu, G. The physicochemical/biological properties of porous tantalum and the potential surface modification techniques to improve its clinical application in dental implantology. *Mat. Sci. Eng. C-Mater* **2015**, *49*, 323–329. [CrossRef] [PubMed]
12. Huang, G.; Pan, S.-T.; Qiu, J.-X. The clinical application of porous tantalum and its new development for bone tissue engineering. *Materials* **2021**, *14*, 2647. [CrossRef] [PubMed]
13. Ji, P.; Liu, S.; Deng, H.; Ren, H.; Zhang, J.; Sun, T.; Xu, K.; Shi, C. Effect of magnetron-sputtered monolayer Ta and multilayer Ti-Zr-Ta and Zr-Ti-Ta coatings on the surface properties of biomedical Ti-6Al-4V alloy. *Mater. Let.* **2022**, *322*, 132464. [CrossRef]
14. Echavarría, A.M.; Rico, P.; Ribelles, J.G.; Pacha-Olivenza, M.A.; Fernández-Calderón, M.-C.; Bejarano-G, G. Development of a Ta/TaN/TaNx (Ag) y/TaN nanocomposite coating system and bio-response study for biomedical applications. *Vacuum* **2017**, *145*, 55–67. [CrossRef]
15. Hee, A.C.; Zhao, Y.; Jamali, S.S.; Bendavid, A.; Martin, P.J.; Guo, H. Characterization of tantalum and tantalum nitride films on Ti6Al4V substrate prepared by filtered cathodic vacuum arc deposition for biomedical applications. *Surf. Coat. Tech.* **2019**, *365*, 24–32. [CrossRef]
16. Ma, G.; Lin, G.; Gong, S.; Liu, X.; Sun, G.; Wu, H. Mechanical and corrosive characteristics of Ta/TaN multilayer coatings. *Vacuum* **2013**, *89*, 244–248. [CrossRef]
17. Lackner, J.; Waldhauser, W.; Major, B.; Morgiel, J.; Major, L.; Takahashi, H.; Shibayama, T. Growth structure and growth defects in pulsed laser deposited Cr–CrNx–CrCxN1− x multilayer coatings. *Surf. Coat. Tech.* **2006**, *200*, 3644–3649. [CrossRef]
18. Zhou, R.; Ju, H.; Liu, S.; Zhao, Z.; Xu, J.; Yu, L.; Qian, H.; Jia, S.; Song, R.; Shen, J. The influences of Ag content on the friction and wear properties of TiCN–Ag films. *Vacuum* **2022**, *196*, 110719. [CrossRef]
19. Ji, X.; Luo, C.; Juan, J.; Zhao, J.; Zhang, Y. Wear Resistance of Fe-Based Amorphous Powder Deposited Coatings in Air, Water, and SBF Solution: Effect of Layer Number. *Tribol. T.* **2022**, *65*, 1–11. [CrossRef]
20. Röder, H.; Hahn, E.; Brune, H.; Bucher, J.-P.; Kern, K. Building one-and two-dimensional nanostructures by diffusion-controlled aggregation at surfaces. *Nature* **1993**, *366*, 141–143. [CrossRef]
21. Gladczuk, L.; Patel, A.; Paur, C.S.; Sosnowski, M. Tantalum films for protective coatings of steel. *Thin Solid Films* **2004**, *467*, 150–157. [CrossRef]
22. Myers, S.; Lin, J.; Souza, R.M.; Sproul, W.D.; Moore, J.J. The β to α phase transition of tantalum coatings deposited by modulated pulsed power magnetron sputtering. *Surf. Coat. Tech.* **2013**, *214*, 38–45. [CrossRef]
23. Colin, J.J.; Abadias, G.; Michel, A.; Jaouen, C. On the origin of the metastable β-Ta phase stabilization in tantalum sputtered thin films. *Acta Mater.* **2017**, *126*, 481–493. [CrossRef]
24. Koch, R.; Hu, D.; Das, A.K. Compressive stress in polycrystalline Volmer-Weber films. *Phys. Rev. Lett.* **2005**, *94*, 146101. [CrossRef] [PubMed]
25. Metikos-Huković, M.; Kwokal, A.; Piljac, J. The influence of niobium and vanadium on passivity of titanium-based implants in physiological solution. *Biomaterials* **2003**, *24*, 3765–3775. [CrossRef] [PubMed]
26. Vereschaka, A.; Tabakov, V.; Grigoriev, S.; Aksenenko, A.; Sitnikov, N.; Oganyan, G.; Seleznev, A.; Shevchenko, S. Effect of adhesion and the wear-resistant layer thickness ratio on mechanical and performance properties of ZrN-(Zr, Al, Si) N coatings. *Surf. Coat. Tech.* **2019**, *357*, 218–234. [CrossRef]

27. Liu, K.; Zhou, Y.; Yin, L.; Shi, Y.; Huang, G.; Liu, X.; Zheng, L.; Xing, Z.; Zhang, X.; Liang, S. Surface Microstructure and Performance of Anodized TZ30 Alloy in SBF Solution. *Metals* **2022**, *12*, 719. [CrossRef]
28. Philippon, D.; Godinho, V.; Nagy, P.; Delplancke-Ogletree, M.; Fernandez, A. Endurance of TiAlSiN coatings: Effect of Si and bias on wear and adhesion. *Wear* **2011**, *270*, 541–549. [CrossRef]
29. Çelik, A.; Aslan, M.; Yetim, A.F.; Bayrak, Ö. Wear behavior of plasma oxidized CoCrMo alloy under dry and simulated body fluid conditions. *J. Bionic. Eng.* **2014**, *11*, 303–310. [CrossRef]
30. Palanivelu, R.; Kumar, A.R. Scratch and wear behaviour of plasma sprayed nano ceramics bilayer Al2O3-13 wt% TiO2/hydroxyapatite coated on medical grade titanium substrates in SBF environment. *Appl. Surf. Sci.* **2014**, *315*, 372–379. [CrossRef]
31. Wang, L.; Zhang, G.; Wood, R.; Wang, S.; Xue, Q. Fabrication of CrAlN nanocomposite films with high hardness and excellent anti-wear performance for gear application. *Surf. Coat. Tech.* **2010**, *204*, 3517–3524. [CrossRef]
32. Sun, S.; Ye, Y.; Wang, Y.; Liu, M.; Liu, X.; Li, J.; Wang, L. Structure and tribological performances of CrAlSiN coatings with different Si percentages in seawater. *Tribol. Int.* **2017**, *115*, 591–599. [CrossRef]
33. Akhter, R.; Zhou, Z.; Xie, Z.; Munroe, P. Enhancing the adhesion strength and wear resistance of nanostructured NiCrN coatings. *Appl. Surf. Sci.* **2021**, *541*, 148533. [CrossRef]
34. Niu, Y.; Chen, M.; Wang, J.; Yang, L.; Guo, C.; Zhu, S.; Wang, F. Preparation and thermal shock performance of thick α-Ta coatings by direct current magnetron sputtering (DCMS). *Surf. Coat. Tech.* **2017**, *321*, 19–25. [CrossRef]
35. Maeng, S.; Axe, L.; Tyson, T.; Gladczuk, L.; Sosnowski, M. Corrosion behaviour of magnetron sputtered α-and β-Ta coatings on AISI 4340 steel as a function of coating thickness. *Corros. Sci.* **2006**, *48*, 2154–2171. [CrossRef]
36. Qin, W.; Fu, L.; Zhu, J.; Yang, W.; Li, D.; Zhou, L. Tribological properties of self-lubricating Ta-Cu films. *Appl. Surf. Sci.* **2018**, *435*, 1105–1113. [CrossRef]
37. Xu, B.; Zhu, Z.; Ma, S.; Zhang, W.; Liu, W. Sliding wear behavior of Fe–Al and Fe–Al/WC coatings prepared by high velocity arc spraying. *Wear* **2004**, *257*, 1089–1095. [CrossRef]
38. Newbury, D.E.; Ritchie, N.W. Is scanning electron microscopy/energy dispersive X-ray spectrometry (SEM/EDS) quantitative? *Scanning* **2013**, *35*, 141–168. [CrossRef]

Disclaimer/Publisher's Note: The statements, opinions and data contained in all publications are solely those of the individual author(s) and contributor(s) and not of MDPI and/or the editor(s). MDPI and/or the editor(s) disclaim responsibility for any injury to people or property resulting from any ideas, methods, instructions or products referred to in the content.